Materials Today Communications 26 (2021) 102110

Contents lists available at ScienceDirect

Materials Today Communications

journal homepage: www.elsevier.com/locate/mtcomm

Reduced graphene oxide decorated with Ni-Fe-Mo permalloy obtained by sputtering

Thuany Garcia Maraschin [a], Samuel Corvello Vilar [a], Dario Eberhardt [a], Adriano Friedrich Feil [a], José Antonio Malmonge [b], Julian Geshev [c], Griselda Barrera Galland [d], Nara Regina de Souza Basso [a,*]

[a] Escola Politécnica, Pontifícia Universidade Católica do Rio Grande do Sul, Av. Ipiranga, 6681, 90619-900, RS, Brazil
[b] Universidade Estadual Paulista, UNESP, Faculdade de Engenharia, Campus de ilha solteira, Av. Brasil 56, 15385-000, SP, Brazil
[c] Instituto de Física, Universidade Federal do Rio Grande do Sul, Av. Bento Gonçalves 9500, 91501-970, RS, Brazil
[d] Instituto de Química, Universidade Federal do Rio Grande do Sul, Av. Bento Gonçalves 9500, 91501-970, RS, Brazil

ARTICLE INFO

Keywords:
Sputtering
Metals and alloys
Nanoparticles
Reduced graphene oxide

ABSTRACT

This work illustrates an effective method for obtaining hybrid nanoparticles of Ni-Fe-Mo permalloy and reduced graphene oxide (rGO). The metallic nanoparticles were spread by the sputtering technique, which allowed a good dispersion of the metallic nanoparticles onto rGO substrate powder. TEM showed permalloy nanoparticles smaller than 8 nm uniformly distributed throughout rGO. Permalloy/rGO hybrid with 10.5 wt% loading of permalloy nanoparticles was calculated by TGA. RBS experiment reveals that permalloy target and the nanoparticles deposited have similar composition. The interaction between permalloy and rGO was studied by FT-IR. Ni-Fe-Mo/rGO presented an electrical conductivity of 122 Scm^{-1}, significantly higher than the original rGO and a magnetization hysteresis-loop coercivity of 16 Oe at room temperature. To our knowledge this is the first work in which permalloy nanoparticles are deposited onto graphene powder substrate by a physical impregnation technique.

1. Introduction

Reduced graphene oxide (rGO) is a very useful derivative of graphene oxide used in numerous multicomponent materials [1]. rGO shows oxygen functionalities that play important roles in the preparation of hybrid materials since the oxygenated atoms support the deposition of metallic nanoparticles onto the rGO surface [2,3].

Hybrid nanoparticles of graphene decorated with metals have been prepared to produce a combination of properties that can be useful in magnetic sensors [4], chemical gas sensors [2], corrosion resistant materials [5], conductive electrodes [6] and catalytic performances [7]. The Ni-Fe-Mo (permalloy) is widely used soft magnetic material owing to its mechanical, electrical, magnetic, and corrosion resistant properties. Furthermore, magnetic nanoparticles deposited on a graphene surface have been predicted to present high magnetoresistance and high conductivity, an important combination of properties for magnetic sensors [3,5].

Metallic graphene hybrids are mainly prepared via a chemical route, which generates hazardous by-products. In a typical experiment, precursors of metallic species are mixed in aqueous solution in reactors, which often require thermal treatment, continuous mechanical stirring, reducing agents, many processing steps and long times [6–8]. Regarding the production of hybrid nanoparticles, sputtering impregnation technique is very versatile because it can result in a wide variety of morphologies and functionalization, besides the absence of toxic chemicals and by-products [9].

The sputtering technique was used previously with graphene to deposit Pt on porous graphene produced by chemical vapor deposition (CVD) process to use as catalyst support for polymer electrolyte membrane (PEM) fuel cells [10]. Titanium (Ti) atoms were sputtered to dope a reduced graphene oxide (rGO) thin film surface to be used as dye-sensitized solar cells [11]. The sputtering deposition of Au NPs onto GO modified with amine-functionalized ionic liquids (ILs) generates promising hybrid materials to be used as efficient biosensors for cholesterol detection [12].

Some examples of permalloy/graphene also exist in literature. FeNi

* Corresponding author.
E-mail address: nrbass@pucrs.br (N.R. de Souza Basso).

https://doi.org/10.1016/j.mtcomm.2021.102110
Received 19 August 2020; Received in revised form 28 January 2021; Accepted 29 January 2021
Available online 3 February 2021
2352-4928/© 2021 Elsevier Ltd. All rights reserved.

alloy nanoparticles (NPs) supported by reduced graphene oxide (rGO) were successfully synthesized through in-situ reduction of iron and nickel salts with hydrazine hydrate [13]. Recently, randomly oriented permalloy nanowires (Py NWs/GO) composites were obtained by decorating multilayered GO thick films with ~30 nm in diameter and 1 μm long. Permalloy nanowires were synthetized by electrodeposition inside anodic aluminium oxide (AAO) templates, while GO sheets were prepared using commercial GO after several cycles of sonication and sequential deposition steps [14]. NiFe alloy nanoparticles embedded in nitrogen-doped graphene layers were successfully fabricated under a mixed gas of $CH_4/N_2/Ar$ [15]. In another study a NiFe alloy nanoparticle/graphene oxide hybrid (NiFe/GO) for electrochemical glucose sensing was obtained. GO was prepared by a modified Hummers' method and the NiFe/GO composite by a mixture of metal salts in aqueous solution [16]. However, to the best of our knowledge, the rGO powder sputtered by permalloy nanoparticles has never been reported.

The present work highlights the use of the magnetron sputtering technique for physical impregnation of permalloy by deposition on a rGO powder substrate at room temperature, a potentially sustainable alternative to conventional chemical methods. The methodology presented here describes the coverage of powder substrates with metallic nanoparticles via an electro-magnetic vibrational device adapted to magnetron sputtering equipment.

In this study, the new hybrid nanomaterial (Ni-Fe-Mo) based on permalloy deposited onto rGO powder substrate was investigated. Transmission electron microscopy (TEM) and selected area electron diffraction SAED, thermogravimetric analyses (TGA), Rutherford backscattering spectrometry (RBS), Fourier transform infrared spectra (FT-IR), electrical conductivity and magnetization measurements were carried out in order to evaluate the hybrid and its properties.

2. Experimental

2.1. Synthesis of Ni-Fe-Mo/rGO

Reduced graphene oxide (rGO) with 10 % oxygen was synthesized from natural graphite by a modified Staudenmaier method as described previously [17,18]. Permalloy nanoparticles were deposited by magnetron sputtering onto rGO substrate at room temperature. Briefly, for sputtering deposition, 0.1 g of rGO powder was placed into a holder cup connected to a mechanical resonant agitator that permits continuous homogenization of the deposited nanoparticles on the entire powder surface. Permalloy nanoparticles were deposited using a permalloy/Hymu 80 target (80.25 wt% Ni, 15.17 wt% Fe and 4.58 wt% Mo, Kurt J. Lesker Company). All sputtering depositions were performed at 50 W under argon (99.99 %, purchased from White Martins - Brazil) with the working pressure set at 2.1×10^{-2} mbar, 120 mm target-to-agitator distance, and 23 min sputtering time, reaching 10 % w/w (mass of permalloy in relation to the rGO), named Permalloy/rGO.

2.2. Characterization

For TEM analysis, the samples remained one hour in ultrasonic bath (45 kHz) in acetone and deposited on copper grid. The TEM images and collect selected area electron diffraction (SAED) patterns were obtained using a Microscope EOL, 2010 operating at 200 kV. Further, nanoparticles were randomly chosen from the TEM image to be measured for metal particle size by ImageJ software. TGA were carried out on a thermogravimetric analyzer (DT Q600; TA Instruments) at a heating rate of 10 °C min^{-1}. The samples were heated from 25 to 800 °C under synthetic air flow rates of 100 mL min^{-1}. For RBS analysis, two samples were made, a pressed permalloy/rGO pellet (1 mm thick) and for comparison, same method was used to obtain a standard sample without rGO where permalloy was deposited on ultrapure silicon (111) slide (permalloy/Si). The deposition time of permalloy on the silicon surface was 20 min. The RBS measurements were carried out in a 3 MV Tandetron accelerator using a He^+ ion beam of 2.0 MeV. The Si surface-barrier detector was positioned at a scattering angle of 165°. The simulations of the spectra related to the samples used were made in the SIMNRA software, for the samples used the first layer was simulated, consisting of the metals Ni, Fe and Mo. According to the technical certification, the permalloy target consists of 80.25 % nickel, 15.17 % iron and 4.58 % molybdenum. Therefore, we used a proportion between these elements close to that of the target. After the simulations, the graphs with the experimental and simulated data for each sample were generated by Origin software. FT-IR of the samples were recorded in the range of 400–4000 cm^{-1} using a Perkin Elmer Instruments Spectrum One spectrometer which accumulated 14 scans. For the FT-IR measurements, samples were mixed with KBr and thereafter, pellets were prepared. The electrical conductivity was measured on pressed rGO and permalloy/rGO pellets (<1 mm thick) with a four-point collinear probe device. A Keithley 236 source measurement unit was employed to provide a constant current and an HP34401 multimeter was used to measure the voltage. The magnetic properties of permalloy/rGO were investigated using an EZ9 MicroSense vibrating sample magnetometer (VSM) at room temperature with a magnetic field (H) cycled between −20 kOe and +20 kOe; this magnitude of H was sufficiently high to avoid minor-loop effects [19,20]. For visual images of the magnetic properties, the samples were dispersed in acetone and an external magnetite were used.

3. Results and discussion

The structural morphology of the material was characterized by TEM. Fig. 1a shows the rGO sheets rippled structure, originated from deformation during graphite oxidation [8]. Permalloy/rGO hybrid TEM micrograph (Fig. 1b) shows permalloy nanoparticles covering homogeneously the surface of the fully exfoliated and almost transparent graphene sheets. As the permalloy/rGO sample was ultrasonicated in a bath during one hour, previously, the remainder of the metallic nanoparticles on rGO indicates an interaction between the rGO and the metal nanoparticles. These results suggest the "fixing effect" of rGO functional groups in the hybrid material. Zhu et al. [21] observed this behavior when nanosized $NiFe_2O_4$ hybrid crystals were obtained with few-layered rGO sheets by in situ hydrothermal route. On the other hand, the TEM of permalloy target (Fig. 1c) without the rGO substrate, the particles tend to aggregate. The inset Fig. 1a–c shows the selected area electron diffraction (SAED) patterns of samples. The graphene (inset Fig. 1a) SAED pattern possesses clear diffraction spots with a six-fold pattern that is consistent with the hexagonal lattice [22]. The d-spacing is 2.10 Å and 1.23 Å. The results show graphene with high crystallization quality. However, since the obtained rGO has ~7−8 layers [18] there is overlapping of the standards. Other research groups exhibit similar results [22–24]. Some materials have a known crystalline structure, as well as their interplanar distances, so a comparison can be made with the distances measured experimentally. However, in the case of a relatively new material, the permalloy does not have such known parameters. A representative SAED pattern obtained from graphene decorated with permalloy nanoparticles is provided in inset Fig. 1b. The diffraction rings in the SAED pattern were calculated as r1 = 2.11 Å and r2 = 1.22 Å close to SAED pattern of rGO, this suggests that the rGO structure is not changed by sputtering permalloy, nevertheless permalloy/rGO diffraction pattern shows rings instead of diffraction spots, indicating a polycrystalline sample [25–27]. The permalloy diffraction rings in the SAED pattern (insert in Fig. 1c) were calculated as r1 = 2.06 Å; r2 = 1.78 Å; r3 = 1.26 Å. Since the permalloy composition is 80.25 % Ni, 15.17 % Fe and 4.58 % Mo, it is possible to compare with Ni_3Fe in which these d-spacing values correspond to (111), (200) and (220) planes [28–30].

Beyond that, 200 nanoparticles randomly chosen from the TEM image have been measured to analyze metal particle size in permalloy/rGO hybrid. The histogram presented in Fig. 1d shows particles with size

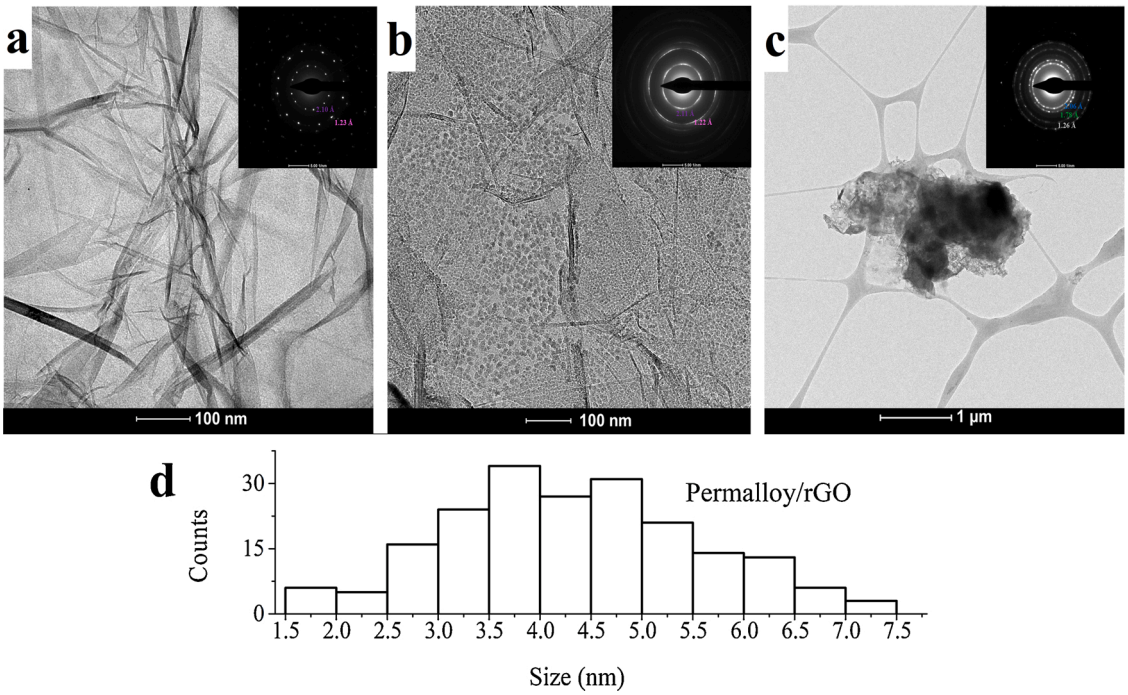

Fig. 1. TEM and SAED (inset images): (a) rGO, (b) permalloy/rGO, (c) Permalloy target. (d) The particle size distribution of permalloy/rGO hybrid.

ranging between 1.5 and 7.0 nm. The absence of aggregates can be a result of the deposition technique used, combined with the presence of oxygenated functional groups on the rGO substrate surface, which could allow the anchoring of the metal nanoparticles [31,32]. This small particle size is remarkable compared with other works. Feng et al. [33] obtained in-situ anchored porous $FeNi_3$ nanocrystals on graphene nanosheets, using one-pot reaction, but the nanospheres had average sizes between 64 and 154 nm, significantly bigger than that obtained by the sputtering method. Sun et al. [13] grew FeNi alloy nanoparticles on rGO by reducing iron and nickel salts with hydrazine hydrate and obtained spheres with diameters between 70−100 nm.

Fig. 2 shows the thermo gravimetric analysis (TGA) profile of samples of permalloy target (a), rGO (b) and permalloy/rGO hybrid (c).

The thermogravimetric profile of permalloy target (Fig. 2a) presents an almost stable curve with a slight weight increase at high temperatures, that is of 1.2 % of the initial weight at 700 °C. As the analysis was performed in air atmosphere, it is possible that some metallic nanoparticles react with oxygen to produce some oxides. The TGA curves of the rGO and permalloy/rGO samples show similar trends (Fig. 2b,c). There is in both cases a sharp decrease in weight resulting from the combustion of carbon atoms in rGO skeleton comprising carbon and oxygen functional groups [34–36]. However, in rGO the initial degradation temperature is of 376 °C ending at 650 °C and in permalloy/rGO initiates at 420 °C and ends at 690 °C showing a stabilization effect of the metals in rGO degradation. The percentage of residues is also different. In rGO it is only 1.6 % of the initial weight due to carbon ashes while in permalloy/rGO it is of 13.3 % and must be composed by carbon from rGO and the alloy metals. If the amount of carbon is discounted from the total quantity of the residue the percentage of metals is attained for the sample. This amount is of 11.7 % and if it is supposed that the metals could increase about 1.2 % of the initial weight due to oxidation reactions it obtains the amount of 10.5 %, very close to the amount of permalloy theoretical sputtered in rGO (10 %).

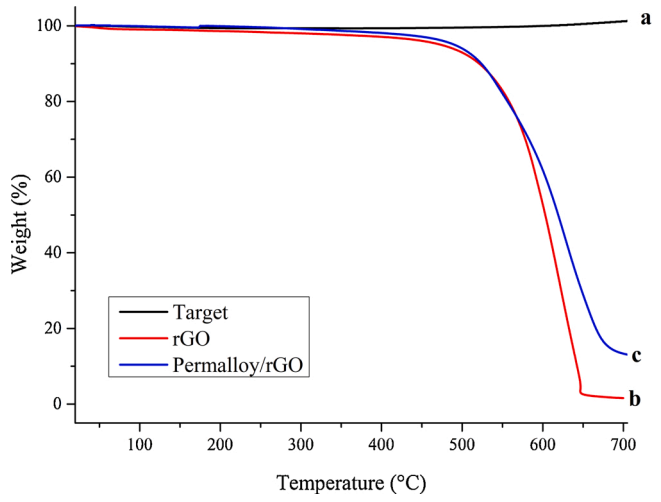

Fig. 2. TGA analysis at a heating rate of 10 °C min^{-1} in air: (a) Permalloy target, (b) rGO and (c) permalloy/rGO hybrid.

The compositions of permalloy/rGO also were investigated by RBS. The sputtered permalloy/Si (Fig. 3a) was used as standard to verify the composition of pure permalloy. The spectrum shows only the peaks related to Ni, Fe and Mo, and the Si which represent the substrate. In Fig. 3b, the percentages of carbon (91.4 %) and oxygen (8.6 %) were close to those used in the simulation, obtained by the rGO elemental analysis (89.7 % C and 10.3 % O) [18]. The S and K elements found in the substrate are due to the graphite oxidation process [37]. Comparing RBS spectra for sputtered samples and analyzing only the relative Ni, Fe and Mo elements percentage in standard (permalloy/Si) and permalloy/rGO samples there are 79.0 and 82.0 % Ni, 14.0 and 18.5 % Fe and 2.5 and 4.0 % Mo, respectively. According to these results, the permalloy was deposited on the rGO with equivalent relative metallic elements as described by the permalloy target certificate (80.25 % Ni, 15.17 % Fe and 4.58 % Mo).

Fig. 4 shows the comparison of FT-IR of pristine rGO and permalloy/rGO.

The FT-IR of the pristine rGO shows a very strong band around 3453 cm^{-1} due to O—H stretching vibration of hydroxyl groups, a band at 1634 cm^{-1} due to C=C stretching and around 1033 cm^{-1} the C—O stretching due to C—OH groups [38]. Other bands typical of graphene

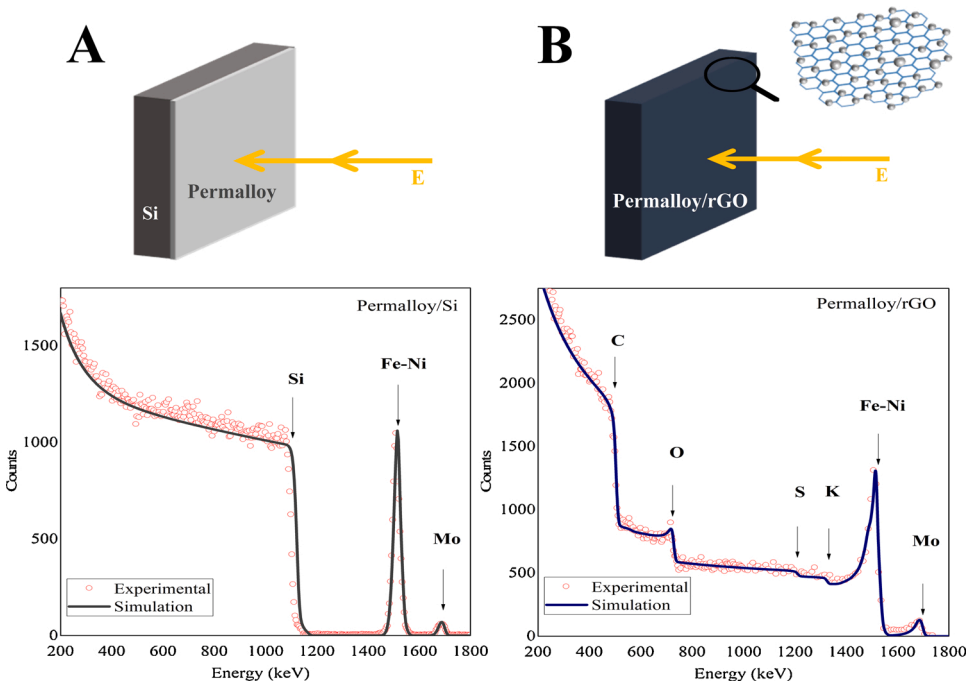

Fig. 3. (a) RBS spectra for sputtered permalloy/Si and (b) permalloy/rGO. The arrow illustrates the energy direction.

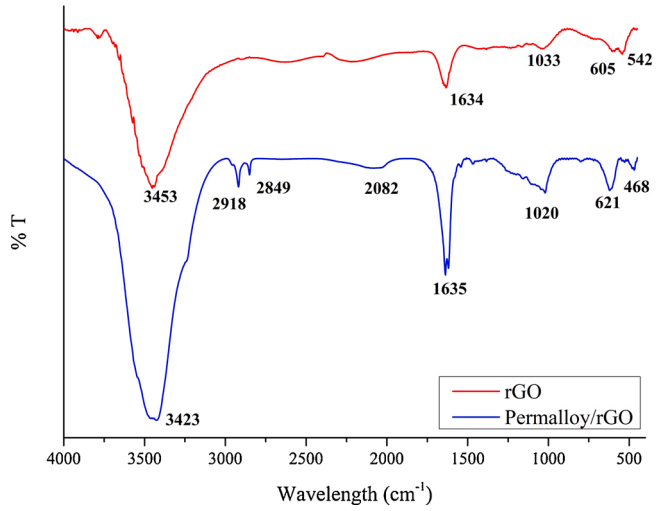

Fig. 4. FT-IR spectra of rGO and permalloy/rGO.

oxide such as carbonyl groups are not observed. The FT-IR spectrum of permalloy/rGO shows differences compared to the spectrum of rGO. The first difference is the increase of the bands due to sp^3 carbon atoms, more specifically it can be observed at 2918 and 2849 cm^{-1} the C—H asymmetric and symmetric stretching, respectively, of methylene groups [38]. The increase of the CH_2 bands would suggest a partial reduction of some aromatic rings of graphene by the catalytic effect of NiFe metals [39]. Finally, another outstanding difference between the spectra of rGO and permalloy/rGO is the clear appearance of two peaks at 621 and 468 cm^{-1}. Bands between 500 and 750 cm^{-1} have been attributed to the stretching of metal—O bond [40]. As there are not references in literature about FT-IR of permalloy sputtered in rGO and the permalloy used in this work is composed mainly of Ni(80 %) and Fe(15 %), a survey was carried out in literature about NiO and FeO stretching's of other compounds containing these metals supported on graphene in which the results differ slightly. In magnetite (Fe_3O_4)/porous graphene nanocomposites the stretching vibration of FeO was observed at 560 cm^{-1} [41] and at 598 cm^{-1} [42]. In FeGO nanocomposites this FeO band was observed as two bands at 694 and 590 cm^{-1} [40]. NiOrGO hybrid showed peaks at approximately 580 cm^{-1} [43] and in graphene nanosheets modified with $Ni(OH)_2$ at 634 cm^{-1}. In both cases they were attributed to NiO stretching. On the other hand, in NiO/graphene aerogel composites the band of NiO stretching vibration was observed at 474 cm^{-1}. Based on this we suggest that the presence of bands at 621 and 468 cm^{-1} in permalloy/rGO nanocomposites can be assigned of NiO and FeO bonds. This suggests a chemical interaction between rGO and metallic nanoparticles. This behavior was also evidenced by TEM.

The permalloy is a very soft magnetic material that possesses notable magnetic properties, as can be seen by the magnetic separation of the particles when an external magnet is applied to a permalloy/rGO nanocomposite acetone suspension. This represents an additional evidence of the immobilization of magnetic nanoparticles over rGO (Fig. 5a). Magnetization $M(H)$ curves of a permalloy/rGO sample are shown in Fig. 5b. The obtained values of the remnant magnetization M_r (normalized to the saturation magnetization M_s of 0.65 emu/g) and the coercive field H_c, are 0.14 and 16 Oe, respectively.

Despite the small amount of magnetic material, the magnetic signal is strong and stable. In order to estimate the effects of magnetic interactions, we employed the recoil-loop interaction plot (δM_R) technique [44]. This method, which exploits a relationship between any recoil loop and the corresponding major hysteresis loop, provides valuable information concerning the magnetic interactions present in the system. For the case of uniaxial anisotropy, any nonzero deviation of $\delta M_R(H)$ should be ascribed to magnetic interactions.

A δM_R plot, constructed from a recoil loop with recoil field equal to H_c, is also plotted in Fig. 5. The rather small $\delta M_R(H)$ plot's values and its shape indicate the presence of very weak dipolar-like interactions stabilizing the demagnetized state. The inset in Fig. 5b shows the low-field range magnetic data obtained on two permalloy/rGO samples, being one of these synthesized approximately two years after the other. The two hysteresis loops are practically indistinguishable (the same holds for the recoil loop and the corresponding δM_R plot, not shown), which demonstrates the very high reproducibility of both synthesis and magnetic properties of the nanoparticles.

The electrical conductivity of permalloy/rGO hybrid species (122

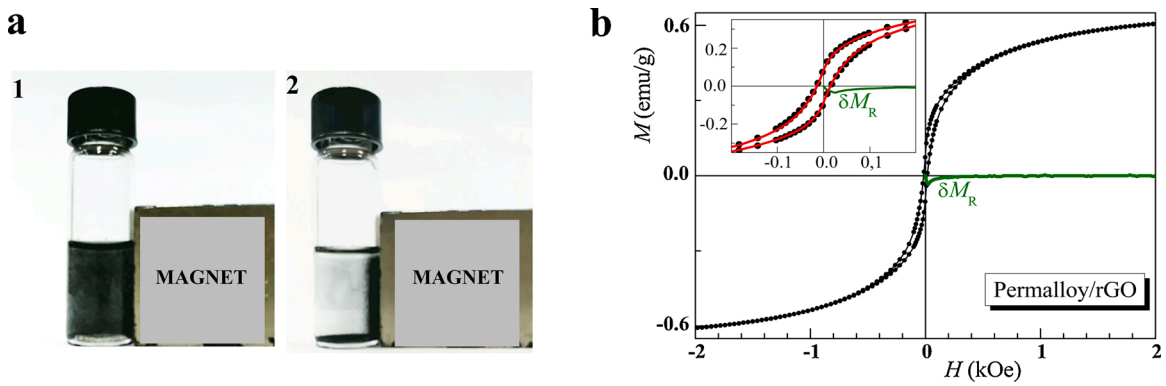

Fig. 5. (a) Visual image of samples with external magnet after 240 s: (1) rGO, (2) permalloy/rGO. (b) Magnetization hysteresis loop of the permalloy/rGO. The inset gives the low-field region where the δM_R plot, constructed from a recoil curve with recoil field equal to H_c is also showed. The solid line in the inset corresponds to a measurement performed on a sample synthesized and characterized magnetically approximately two years after the other (symbols).

Scm^{-1}) was twice that of rGO (60 Scm^{-1}). In the composite, the electrically conductive behavior can be understood from the microstructure. When the volume fraction of the conductive filler reaches percolation, the filler forms a directly-connected network and charge carriers can move through this network. However, an increase in conductivity may occur before percolation due to the hopping and tunneling process of the charge carriers between the neighboring conductive fillers [45,46]. In our case, good dispersion of the metallic nanoparticles (as indicated by the weak interactions, see Fig. 3) on the surface of the rGO was observed and the increase of the electrical conductivity related to rGO was attributed to hopping and tunneling processes of the charge carriers among the nanoparticles.

4. Conclusions

A new powder permalloy/rGO hybrid nanocomposite was successfully prepared through sputtering, avoiding the complications and drawbacks of methods based on chemical functionalization. Compared to the commonly-used chemical routes to depositing metals over a substrate, sputtering allows the deposition of metallic nanoparticles faster with fewer steps and produces no by-products. The technique was used for immobilizing permalloy based Ni-Fe-Mo on a solid substrate, rGO powder, to yield well-distributed nanoparticles instead of aggregates. TEM images showed uniform and homogeneously dispersed spherical permalloy nanoparticles anchored onto the surface of the rGO sheets even after an ultrasound treatment. TGA showed that it is possible to obtain through this technique the desired amount of permalloy on rGO. FT-IR studies suggest a chemical interaction between permalloy and rGO. A small amount of magnetic material can generate a strong and stable signal and improve electrical conductivity. The permalloy/rGO system proved to be very stable and its synthesis and magnetic properties highly reproducible. This new hybrid material can act as nano adsorbents in wastewater treatment and as filler in a polymeric matrix for electromagnetic interference shielding applications.

Declaration of Competing Interest

The authors report no declarations of interest.

Acknowledgments

This research was supported by the Brazilian agencies Conselho Nacional de Desenvolvimento Científico e Tecnológico (grants 302267/2017-4, 305796/2016-0, 422740/2018-7 and 307580/2018-0) and Coordenação de Aperfeiçoamento de Pessoal de Nível Superior (Finance Code 001).

References

[1] M. Gocyla, M. Pisarek, M. Holdynski, M. Opallo, Electrochem. Commun. 96 (2018) 77–82.
[2] S. Aslam, T.H. Bokhari, T. Anwar, U. Khan, A. Nairan, K. Khan, Mater. Lett. 235 (2019) 66–70.
[3] K.A. Deepthi, R. Balachandran, B.H. Ong, K.B. Tan, H.Y. Wong, H.K. Yow, S. Srimala, Appl. Surf. Sci. 360 (2016) 519–524.
[4] M. Nisar, C.P. Bergmann, J. Geshev, R. Quijada, T. Maraschin, N.R. de Souza Basso, E.G. Barrera, G.B. Galland, J. Appl. Polym. Sci. 134 (2017) 1–7.
[5] A.K. Chaudhari, V.B. Singh, J. Alloys Compd. 751 (2018) 194–214.
[6] X. Chen, Q. Ru, Z. Wang, X. Hou, S. Hu, Mater. Lett. 191 (2017) 218–221.
[7] L. Wang, Y. Zhang, Z. Li, Mater. Lett. 94 (2013) 179–182.
[8] Y. lei, Z. Yao, H. Lin, A. Ali Haidry, J. Zhou, P. Liu, Mater. Lett. 236 (2019) 456–459.
[9] M.T. Nguyen, T. Yonezawa, Sci. Technol. Adv. Mater. 19 (2018) 883–898.
[10] M.S. Yazici, M.A. Azder, O. Salihoglu, F.G. Boyaci San, Int. J. Hydrogen Energy 43 (2018) 18572–18577.
[11] F.W. Low, C.W. Lai, N. Asim, M. Akhtaruzzaman, M. Alghoul, S.K. Tiong, N. Amin, Sol. Energy 188 (2019) 10–18.
[12] N.M. Galdino, G.S. Brehm, R. Bussamara, W.D.G. Gonçalves, G. Abarca, J. D. Scholten, J. Mater. Chem. B 5 (2017) 9482–9486.
[13] C. Sun, W. Jiang, Y. Wang, D. Sun, J. Liu, P. Li, F. Li, Phys. Status Solidi - Rapid Res. Lett. 8 (2014) 141–145.
[14] D.M.A. Jaimes, P. Márquez, A. Ovalle, J. Escrig, O.L. Pérez, N. Bajales, Sci. Rep. 10 (2020) 1–13.
[15] X. Qu, Y. Zhou, X. Li, M. Javid, F. Huang, X. Zhang, X. Dong, Z. Zhang, Inorg. Chem. Front. 7 (2020) 1148–1160.
[16] Z.P. Deng, Y. Sun, Y.C. Wang, J. De Gao, Sensors (Switzerland) 18 (2018) 1–12.
[17] G. Pavoski, T. Maraschin, F. de C. Fim, N.M. Balzaretti, G.B. Galland, C.S. Moura, N.R. de S. Basso, Mater. Res. 20 (2017) 53–61.
[18] T.G. Maraschin, R. da S. Correa, L.F. Rodrigues, N.M. Balzarettid, J.A. Malmonge, G.B. Galland, N.R. de S. Basso, Mater. Res. 22 (2019) 1–10.
[19] J. Geshev, J. Magn. Magn. Mater. 467 (2018) 135–138.
[20] J. Geshev, J. Phys. Condens. Matter 21 (2009), 078001.
[21] P. Zhu, S. Liu, J. Xie, S. Zhang, G. Cao, X. Zhao, J. Mater. Sci. Technol. 30 (2014) 1078–1083.
[22] K. Krishnamoorthy, M. Veerapandian, K. Yun, S.J. Kim, Carbon N. Y. 53 (2013) 38–49.
[23] J. Liu, Q. Ma, Z. Huang, G. Liu, H. Zhang, Adv. Mater. 31 (2019), 1800696.
[24] H. Zhang, F. Ding, H. Li, F. Qu, H. Meng, H. Gu, Mater. Lett. 244 (2019) 171–174.
[25] Z. Hu, G. Tong, D. Lin, Q. Nian, J. Shao, Y. Hu, M. Saei, S. Jin, G.J. Cheng, J. Mater. Process. Technol. 231 (2016) 143–150.
[26] R.D. Souza, T. Vats, A. Chattree, P.F. Siril, Catal. Letters 148 (2018) 2848–2855.
[27] M.Y. Rekha, N. Mallik, C. Srivastava, Sci. Rep. 8 (2018) 1–10.
[28] D.G. Tong, D.M. Tang, W. Chu, G.F. Gu, P. Wu, J. Mater. Chem. A 1 (2013) 6425–6432.
[29] C.-T. Hsieh, C.-L. Huang, Y.-A. Chen, S.-Y. Lu, Appl. Catal. B Environ. 267 (2020), 118376.
[30] D. Liu, R. Qiang, Y. Du, Y. Wang, C. Tian, X. Han, J. Colloid Interface Sci. 514 (2018) 10–20.
[31] V. Georgakilas, J.N. Tiwari, K.C. Kemp, J.A. Perman, A.B. Bourlinos, K.S. Kim, R. Zboril, Chem. Rev. 116 (2016) 5464–5519.
[32] S. Gurunathan, J.W. Han, J.H. Park, E. Kim, Y.J. Choi, D.N. Kwon, J.H. Kim, Int. J. Nanomedicine 10 (2015) 6257–6276.
[33] J. Feng, Y. Zong, Y. Sun, Y. Zhang, X. Yang, G. Long, Y. Wang, X. Li, X. Zheng, Chem. Eng. J. 345 (2018) 441–451.
[34] H. Beygi, A. Babakhani, J. Magn. Magn. Mater. 421 (2017) 177–183.
[35] H. Qiu, F. Qiu, X. Han, J. Li, J. Yang, Appl. Surf. Sci. 407 (2017) 509–517.
[36] J. Li, D. Zhang, H. Qi, G. Wang, J. Tang, G. Tian, A. Liu, H. Yue, Y. Yu, S. Feng, RSC Adv. 8 (2018) 8393–8401.
[37] P.P. Brisebois, M. Siaj, J. Mater. Chem. C 8 (2020) 1517–1547.

[38] D.L. Pavia, G.M. Lampman, G.S. Kriz, J.A. Vyvyan, Introduction to Spectroscopy, 4th ed., Cengage Learning, 2009.
[39] D. Shi, R. Wojcieszak, S. Paul, E. Marceau, Catalysts 9 (2019) 451.
[40] C. Zhang, X. Fu, X. Zhang, J. Li, X. Fan, G. Zhang, Nanomaterials 10 (2020) 144.
[41] G. Bharath, E. Alhseinat, N. Ponpandian, M.A. Khan, M.R. Siddiqui, F. Ahmed, E. H. Alsharaeh, Sep. Purif. Technol. 188 (2017) 206–218.
[42] R. Balasubramanian, S. Chowdhury, J. Mater. Chem. A 3 (2015) 21968–21989.
[43] Y.-L.T. Ngo, S.H. Hur, Mater. Res. Bull. 84 (2016) 168–176.
[44] A. Harres, M. Mikhov, V. Skumryev, A.M.H. De Andrade, J.E. Schmidt, J. Geshev, J. Magn. Magn. Mater. 402 (2016) 76–82.
[45] P.V. Rebeque, M.J. Silva, C.R. Cena, H.N. Nagashima, J.A. Malmonge, D.H. F. Kanda, Polym. Compos. 40 (2019) 7–15.
[46] A.J. Marsden, D.G. Papageorgiou, C. Vallés, A. Liscio, V. Palermo, M.A. Bissett, R. J. Young, I.A. Kinloch, 2D Mater. 5 (2018), 032003.